Lyapunov spectra and conjugate-pairing rule for confined atomic fluids

Bernadi, Stefano; Todd, B.D.; Hansen, Jesper Schmidt; Searles, Debra J.; Frascoli, Federico

Published in:
Journal of Chemical Physics

DOI:
10.1063/1.3446809

Publication date:
2010

Document Version
Publisher's PDF, also known as Version of record

Lyapunov spectra and conjugate-pairing rule for confined atomic fluids

Stefano Bernardi,[1,a)] B. D. Todd,[1,b)] J. S. Hansen,[2] Debra J. Searles,[3,c)] and Federico Frascoli[4]
[1]*Centre for Molecular Simulation, Swinburne University of Technology, Hawthorn, Victoria 3122, Australia*
[2]*DNRF Center "Glass and Time," IMFUFA, Roskilde University, Roskilde DK-4000, Denmark*
[3]*Queensland Micro- and Nanotechnology Centre and School of Biomolecular and Physical Sciences, Griffith University, Brisbane Qld 4111, Australia*
[4]*Brain Sciences Institute, Swinburne University of Technology, Hawthorn, Victoria 3122, Australia*

(Received 16 February 2010; accepted 17 May 2010; published online 24 June 2010)

In this work we present nonequilibrium molecular dynamics simulation results for the Lyapunov spectra of atomic fluids confined in narrow channels of the order of a few atomic diameters. We show the effect that realistic walls have on the Lyapunov spectra. All the degrees of freedom of the confined system have been considered. Two different types of flow have been simulated: planar Couette flow and planar Poiseuille flow. Several studies exist on the former for homogeneous flows, so a direct comparison with previous results is performed. An important outcome of this work is the demonstration of how the spectrum reflects the presence of two different dynamics in the system: one for the unthermostatted fluid atoms and the other one for the thermostatted and tethered wall atoms. In particular the Lyapunov spectrum of the whole system does not satisfy the conjugate-pairing rule. Two regions are instead distinguishable, one with negative pairs' sum and one with a sum close to zero. To locate the different contributions to the spectrum of the system, we computed "approximate" Lyapunov exponents belonging to the phase space generated by the thermostatted area and the unthermostatted area alone. To achieve this, we evolved Lyapunov vectors projected into a reduced dimensional phase space. We finally observe that the phase-space compression due to the thermostat remains confined into the wall region and does not significantly affect the purely Newtonian fluid region. © *2010 American Institute of Physics*.
[doi:10.1063/1.3446809]

I. INTRODUCTION

Lyapunov exponents measure the average rate of expansion or contraction of the distance between infinitesimally displaced phase space trajectories in a dynamical system. They are one of the main tools for the characterization of chaos, providing a quantitative measure of the chaoticity of the system. A dynamical system is defined to be chaotic if at least one of its Lyapunov exponents is positive. Lyapunov spectra have been computed for several smooth and continuous dynamical systems in the past, either for equilibrium or nonequilibrium steady states, see, for example, Refs. 1 and 2. They have proven to be a particularly useful tool for the characterization and theoretical analysis of systems far from equilibrium in thermostatted steady states. Furthermore, it is possible to use the exponents to derive an expression for quantifying the probability of observing violations of the second law of thermodynamics; this is known as the fluctuation theorem (FT).[3–6] The FT explains Loschmidt's paradox which questions the possibility of obtaining irreversibility from time-reversible dynamics. One of the first models showing the emergence of irreversibility in steady states with time-reversible dynamics is the Galton board model,[7] describing the motion of a particle through a periodic array of scatterers. Studies of this model revealed the multifractal structure of the phase space with the presence of a repellor-attractor pair. The repellor is characterized by an expanding phase-space volume and positive Lyapunov exponent sum, and the attractor is characterized by a contracting phase-space volume, negative Lyapunov exponent sum, and a dimensionality lower than the full phase space (due to the dissipative dynamics).[8]

The study of the Lyapunov spectra is interesting not only for characterizing dynamical instabilities and the geometry of the phase space,[9,10] but also because it provides a link between dynamical systems theory and statistical mechanics. It has been shown that many transport properties of fluids are related to the Lyapunov exponents. More precisely, for thermostatted systems in nonequilibrium steady states, the rate of entropy production can be related to the sum over the Lyapunov exponents and then to the transport coefficients.[11,12] This is true in general and is valid even for nonlinear processes far from equilibrium.[13,14] Furthermore, if the system satisfies the so-called conjugate pairing rule (CPR), the transport coefficients can be computed by knowing only the maximal exponents. The CPR states that if the Lyapunov exponents are ordered from the largest to the smallest ($\lambda^1 > \lambda^2 \cdots > \lambda^M$), where M is the phase space dimension of the system, one finds that the sums of the ordered couples ($\lambda^n + \lambda^{M+1-n}$, $n=1, M/2$) are a constant.[12,14,15] In this paper we define the exponent pair index such that it is maxi-

[a)]Electronic mail: sbernardi@ict.swin.edu.au.
[b)]Electronic mail: btodd@swin.edu.au.
[c)]Electronic mail: d.bernhardt@griffith.edu.au.

mum for the maximum (in absolute value) Lyapunov exponents. Exponent pair index$=M/2-1+n$. For Hamiltonian systems the CPR is always true and the couples sum to zero due to their symplectic nature. While one particular Lyapunov exponent measures the expansion or contraction in a particular direction of the phase space, the sum quantifies what happens to the entire hypervolume. Thus Hamiltonian systems, being volume preserving, show exponents that sum to zero. Several studies have been made to determine which conditions are sufficient for CPR to hold,[13,15–18] but so far the focus has been on homogeneous systems in which the equations of motion are modified to include external forces and thermostatting terms. Systems whose unthermostatted equations of motion are symplectic will obey the CPR, provided that an appropriate thermostatting mechanism is selected and distributes the dissipation equally among all degrees of freedom. Such systems are referred to as μ-symplectic.[15]

In this work we characterize Lyapunov spectra for inhomogeneous systems in nonequilibrium steady states, thereby obtaining an insight into what happens along different directions in the phase space characterized by different dynamics. We focus on two types of flow, namely, planar Couette and Poiseuille flows. The former describes the motion of a fluid confined between two surfaces moving with equal and opposite velocities, the latter a fluid flow inside a channel under the influence of an external force field (e.g., gravity) or pressure gradient.

These types of flows have been investigated extensively in nonequilibrium molecular dynamics, and in the case of Couette flow, either for homogeneous or inhomogeneous systems. They are in fact relatively simple to model and provide a detailed understanding of the rheological properties of fluids in such states. Research on these types of flow is important in many areas (biological, biomedical, micro- and nanofluidics, turbulence, etc.), and in industrial applications, largely in materials science.[19]

The main approach employed to study Couette flow makes use of modified equations of motion (the so-called SLLOD equations of motion),[20] which induce a linear velocity profile, in conjunction with appropriate periodic boundary conditions (PBCs) in the direction perpendicular to the velocity gradient that maintains the correct profile (such as Lees–Edwards PBCs).[21] This approach permits the study of homogeneous systems and extrapolation of bulk properties without introducing surface effects due to the presence of real walls. This saves a huge amount of simulation time by drastically reducing the number of particles involved. The SLLOD equations of motion developed by Evans and Morriss,[20] and derived from a previous set of equations suggested by Hoover *et al.*[22] named DOLLS, give the correct nonlinear response for shear flow. It should be stressed that the SLLOD equations of motion cannot be derived from a Hamiltonian.[23] Even though the equations of motion are not μ-symplectic, departures from the CPR are small for Weeks–Chandler–Anderson (WCA) fluids[24,25] with strain rates less than $\dot{\gamma}\approx 1.0$ in Lennard-Jones reduced units,[14–16,26] and it has been shown to go as $\dot{\gamma}^4$ for a hard sphere gas.[27] Not many studies considered inhomogeneous systems from the point of view of dynamical systems theory, even if historically this has been the first approach that was tried for computing transport properties. In recent years, some work has been carried out to compute the Lyapunov spectra for inhomogeneous systems,[28–32] where models were composed of two regions, one purely Newtonian and one in which the particles were thermostatted. However, these systems were characterized by fewer degrees of freedom and a real comparison with previous results for homogeneous systems was difficult. Our work aims at significantly expanding upon these investigations.

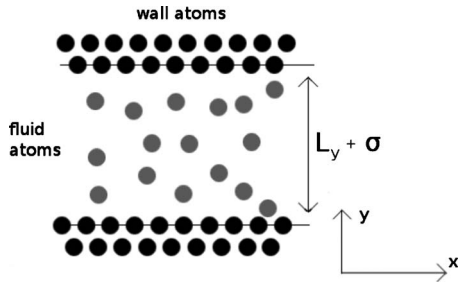

FIG. 1. Schematic of the simulation box for Couette and Poiseuille flows.

II. METHODOLOGY

Our model is a two dimensional atomic fluid flowing in a narrow channel with a width of the order of a few atomic diameters. The channel is periodic in the x-direction and the walls are composed of particles of the same species as that of the fluid (see Fig. 1). The particles (both fluid and wall particles) interact with each other by a smooth repulsive potential, the WCA potential,[24,25] which is a truncated and shifted form of the Lennard-Jones (LJ) potential,

$$\Phi_{WCA} = \begin{cases} 4\epsilon\left[\left(\frac{\sigma}{r_{ij}}\right)^{12} - \left(\frac{\sigma}{r_{ij}}\right)^{6}\right] + \epsilon, & r_{ij} \leq 2^{1/6}\sigma \\ 0, & r_{ij} > 2^{1/6}\sigma, \end{cases} \quad (1)$$

where $r_{ij}=|\mathbf{q_i}-\mathbf{q_j}|$ with $\mathbf{q}_i$ being the laboratory particle position, σ is the value of r_{ij} for which the LJ interaction potential is zero, and ϵ is the well depth of the LJ potential. All the physical units are expressed in reduced units where the unit of mass is the particle mass m, the energy unit is the parameter ϵ, and the length unit is σ. In our work we set $\epsilon=\sigma=m=1$.

In addition to their WCA interactions, the wall particles are subject to a harmonic potential, which tethers each of them to a virtual lattice site, leaving them free to oscillate as a consequence of interactions,

$$\Phi_H(|\mathbf{q}_i^W - \mathbf{q}_i^L|) = \tfrac{1}{2}k_w|\mathbf{q}_i^W - \mathbf{q}_i^L|^2, \quad (2)$$

where the superscripts W and L indicate the wall particle and its lattice site, respectively. The harmonic spring constant k_w has been set to 150, a common value in the literature (see, for example, Travis *et al.*).[33] A shift of the lattice sites drives the wall particles in the case of Couette flow,

$$\Delta q_{ix}^{L} = \pm \tfrac{1}{2}\dot{\gamma} L_y \Delta t, \tag{3}$$

where q_{ix}^{L} is the x coordinate of the lattice site, $\dot{\gamma}$ is the strain rate, $L_y+\sigma$ is the distance between the two walls, as defined in Fig. 1, and Δt is the time step.

A. Thermostat

Because work is performed on the system (in the form of an external field for Poiseuille flow or a shear force for Couette flow) heat must be removed to keep the system at a steady state. Depending on the Lyapunov spectrum we were looking at, a thermostat has been applied either to the fluid, to the walls, or both. The choice of the thermostat is a very crucial point and the definition of temperature itself is an open problem for nonequilibrium systems.[34] Usually the choice lies between either the isokinetic Gaussian[35] or Nosé–Hoover (NH) (Ref. 36) thermostats. The former relies on Gauss' principle of least constraint to make the kinetic energy a constant of motion; the latter uses an integral feedback to keep the average value of kinetic energy fixed (*NVT* versus isokinetic ensemble).

In this work a NH thermostat has been employed mainly because it has the advantage of reproducing the canonical phase-space distribution in the undriven case.[36] It is however not a common choice when computing Lyapunov exponents because it increases the phase space dimension by one for each friction term. It is worth stressing that the effects that a NH thermostat has on the dynamics are different from those of a Gaussian thermostat (which has been more commonly used in simulations of Lyapunov exponents) to avoid any confusion later in the paper. A Gaussian thermostat restricts the dynamics to an isokinetic hypersurface, decreasing the accessible phase space dimension by one. This in turn generates a zero exponent associated with the direction perpendicular to the hypersurface. A NH thermostat, however, does not create a hypersurface, instead it uses an integral feedback mechanism that leaves the temperature free to oscillate around the mean value. There are no vanishing exponents associated with this constraint. The dynamics of its friction coefficient, however, is generated by a first order ordinary differential equation (ODE), which coupled to the particles' ODEs increase the phase space dimension by one. The perturbation vector parallel to this additional direction will generate an extra Lyapunov exponent and our calculations show that its associated Lyapunov exponent has a value close to zero. In this work the two walls confining the fluid are thermostatted independently; therefore, the dimension of the phase space is incremented by two, creating two additional almost vanishing Lyapunov exponents. In the case where the NH thermostat is applied, the equations of motion for the wall particles are given by

$$\dot{\mathbf{q}}_i^{W} = \mathbf{p}_i^{W}/m_i^{W}, \tag{4}$$

$$\dot{\mathbf{p}}_i^{W} = \mathbf{F}_i^{W} - \xi^{W}\mathbf{p}_i^{W}, \tag{5}$$

$$\dot{\xi}^{W} = \frac{1}{Q}\left[\sum_i \frac{\mathbf{p}_i^{W^2}}{m_i^{W}} - N_f k_B T\right], \tag{6}$$

where i is the particle index, the superscript W means that the particle belongs to the wall, Q is a fictitious mass of the heat reservoir, N_f is the number of degrees of freedom, and T is the target temperature. The equations of motion for the fluid particles are

$$\dot{\mathbf{q}}_i^{F} = \mathbf{p}_i^{F}/m_i^{F}, \tag{7}$$

$$\dot{\mathbf{p}}_i^{F} = \mathbf{F}_i^{F} + \mathbf{F}_E, \tag{8}$$

where $\mathbf{F}_E$ is the external force, which is only present for Poiseuille flow. In the case of Couette flow, the walls are moved with equal and opposite velocities by changing the lattice positions, as described above. This generates the fluid motion.

B. Density, temperature, and stress profiles

We compute most fluid properties as a function of the distance from the wall in bins of width Δ. In the bin method we divide the pore into several slabs aligned with the wall direction and compute the averages for every slab/bin of the quantity of interest. This method is very easy to implement but the bin dimension has to be chosen carefully. If it is too wide the resolution will be poor, while if it is too small, few particles will be found in the bin at any time, resulting in poor statistics. An alternative "method of planes" technique (that is exact) can also be used to avoid this ambiguity.[37] Formally, the presence in a bin of a particle at $\mathbf{r}_i$ can be expressed by integrating a Dirac delta function $\delta(\mathbf{r}-\mathbf{r}_i)$ over all positions $\mathbf{r}$ within the bin. The mass density in the position $\mathbf{r}$ and at time t is defined as

$$\rho(\mathbf{r},t) = \sum_i m_i \delta(\mathbf{r} - \mathbf{r}_i(t)), \tag{9}$$

and the streaming velocity as

$$u(\mathbf{r},t) = \frac{\Sigma_i m_i \mathbf{v}_i(t)\,\delta(\mathbf{r} - \mathbf{r}_i(t))}{\Sigma_i m_i \delta(\mathbf{r} - \mathbf{r}_i(t))}. \tag{10}$$

The kinetic temperature has been computed in each bin as[38]

$$\langle T(y_{\text{bin}})\rangle = \frac{\left\langle \Sigma_{i\in \text{bin}}^{N_{\text{bin}}} m_i [\mathbf{v}_i(t) - \mathbf{u}(y,t)][\mathbf{v}_i(t) - \mathbf{u}(y,t)] \right\rangle}{\langle 2N_{\text{bin}}\rangle k_B}, \tag{11}$$

where $\mathbf{v}_i(t)$ is the laboratory velocity of particle i at time t and N_{bin} is the number of particles in any particular bin.

Because of the reduced dimension of the system and the difficulty in defining an instantaneous streaming velocity for each bin at each time step, a running average of the streaming velocity has been used. For the computation of the pressure tensor, we employ the method of planes[39] mentioned above. The pressure tensor can be split into a kinetic and a potential part, $\mathsf{P}=\mathsf{P}^{U}+\mathsf{P}^{K}$. The channel is divided into planes equally spaced, and the velocity of the particles crossing the planes and the force between the particles on opposite sides

of the planes are coupled to generate the potential and kinetic components of the pressure tensor, respectively,

$$P^U_{\alpha y}(y) = \frac{1}{2A}\sum_{ij} F_{\alpha ij}[\Theta(y_i - y)\Theta(y - y_j) - \Theta(y_j - y)\Theta(y - y_i)], \tag{12}$$

$$P^K_{\alpha y}(y) = \lim_{\tau\to\infty} \frac{1}{A\tau} \sum_{0<t_{i,m}<\tau} \sum_i p_{\alpha i}(t_{i,m})\mathrm{sgn}[p_{yi}(t_{i,m})], \tag{13}$$

where i and j are the particle indices, α is any of the x, y, or z components in the force and momentum vectors, Θ is the Heaviside step function, and m indices the times at which the particle crosses the plane. This method allows a high resolution because, unlike the bin method, the separation of the planes does not influence the statistical precision of the pressure tensor.

C. Lyapunov exponents

The motion of the particles in phase space can be determined from the time evolution of the phase vector $\mathbf{\Gamma}(t)=[\mathbf{q}(t),\mathbf{p}(t),\xi(t)]^T$, where $\mathbf{q}(t)=\mathbf{q}_1(t),\ldots,\mathbf{q}_N(t)$, $\mathbf{p}(t)=\mathbf{p}_1(t),\ldots,\mathbf{p}_N(t)$, and $\xi(t)$ represents the variables associated with the thermostatting term if necessary. This can be formally written as

$$\dot{\mathbf{\Gamma}}(t) = \mathbf{G}(\mathbf{\Gamma},t). \tag{14}$$

We can now define a displacement vector $\delta\mathbf{\Gamma}$ as the difference of two phase space vectors. If we take the limit for the displacement vector $\delta\mathbf{\Gamma}\to 0$, this becomes a tangent vector and its motion evolves according to

$$\delta\dot{\mathbf{\Gamma}}(t) = \mathsf{T}\cdot\delta\mathbf{\Gamma}, \tag{15}$$

where T is the stability or Jacobian matrix $\mathsf{T}\equiv\partial\dot{\mathbf{\Gamma}}/\partial\mathbf{\Gamma}$. The formal solution to this linear differential equation is

$$\delta\mathbf{\Gamma}(t) = \mathsf{L}(t)\cdot\delta\mathbf{\Gamma}(0), \tag{16}$$

where

$$\mathsf{L}(t) = \exp_L\left(\int_0^t ds\mathsf{T}(s)\right), \tag{17}$$

and $\exp_L$ is the left time ordered exponential.

The Lyapunov exponents can be defined[40] as

$$\lambda^n = \lim_{t\to\infty}\frac{1}{2t}\ln(\text{eigenvalues}(\mathsf{L}^T(t)\cdot\mathsf{L}(t))). \tag{18}$$

For $n=1,2,\ldots,(2dN+B)$, where d is the Cartesian dimensionality, N is the total number of particles (wall and fluid), and B is the number of additional degrees of freedom introduced by the thermostatting mechanism. It can be shown that an equivalent definition for the Lyapunov exponents is given by considering a set of orthogonal displacement vectors $\delta\mathbf{\Gamma}^n$ that evolve according to Eq. (16), with the addition of a constraint that keeps $\delta\mathbf{\Gamma}^m$ orthogonal to all vectors with $n<m$. In this case the Lyapunov exponents are given by

$$\lambda^n = \lim_{t\to\infty}\lim_{\delta\mathbf{\Gamma}\to 0}\frac{1}{t}\ln\left(\frac{|\delta\mathbf{\Gamma}^n(t)|}{|\delta\mathbf{\Gamma}^n(0)|}\right), \tag{19}$$

where $|\delta\mathbf{\Gamma}^n(t)|$ is the length of the nth orthogonal displacement vector at time t. Since the vectors $\delta\mathbf{\Gamma}^n$ will align with the eigenvectors of $(\mathsf{L}^T(t)\cdot\mathsf{L}(t))$ [see Eq. (18)] after a transient period, they are often referred to as Lyapunov vectors.

Definition equation (19) is more suitable for numerical calculations because some elements of $\mathsf{L}^T(t)\cdot\mathsf{L}(t)$ grow very rapidly. Benettin *et al.*[41–43] developed an algorithm for determining the Lyapunov spectrum of many particle systems using this definition. It evolves a set of tangent vectors in the linearized space (each with an associated Lyapunov exponent) and computes the Lyapunov spectrum by averaging the rate of expansion or contraction of the vectors. Periodic rescaling and orthogonalization are needed to ensure that the limiting behavior $(\lim_{\delta\mathbf{\Gamma}\to 0})$ and orthogonality are maintained. The orthonormalization is performed using the Gram–Schmidt procedure every few time steps. A similar algorithm[44,45] uses Lagrange multipliers to ensure that these constraints are met. Both algorithms were used for comparison in early stages of the work and they produced the same results within statistical error. The Benettin algorithm was then used to obtain the results presented in this work.

In addition to the full Lyapunov spectrum defined above, it is of interest to consider how different parts of the system contribute to the spectrum. In the past, some projections have been considered.[32] In the system studied here, the natural division of the full system into a wall and fluid region, where the dynamics is quite different, suggested consideration of the behavior of subsystem specific exponents. In order to do this, we define displacement vectors $\delta\mathbf{\Gamma}^n_{i\cdots j}\equiv[\delta\mathbf{\Gamma}^n_i,\ldots,\delta\mathbf{\Gamma}^n_j]$, where $\delta\mathbf{\Gamma}^n_i=[\delta\mathbf{q}^n_i,\delta\mathbf{p}^n_i]$ gives the components of the nth displacement vector associated with the ith particle and the displacement vectors associated with all other particles are set to zero. Therefore, we define the subsystem Lyapunov exponents as

$$\lambda^n_{W/F} = \lim_{t\to\infty}\lim_{\delta\mathbf{\Gamma}^n_{i\cdots j}\to 0}\frac{1}{t}\ln\left(\frac{|\delta\mathbf{\Gamma}^n_{i\cdots j}(t)|}{|\delta\mathbf{\Gamma}^n_{i\cdots j}(0)|}\right), \tag{20}$$

where the particle indices $i\cdots j$ are the wall particles for λ^n_W and the fluid particles for λ^n_F. Physically, this can be interpreted as looking at the evolution, in phase space, of the full displacement vector, subject to the constraint that it remains in the reduced space of the subsystem. Note that the dynamics of the subsystem of interest is fully coupled to that of the rest of the system. In this paper we will show how the Lyapunov exponents determined by Eq. (19) are related to those of the subsystem.

To further investigate how the exponents can be associated with distinctive parts of the system, we consider the so-called localization width, as introduced by Taniguchi and Morriss.[46] In this case, instead of looking at the Lyapunov exponents, we consider the corresponding Lyapunov vectors. If the Lyapunov vectors are localized in the phase space, it is possible to say how many and which type of particle contrib-

ute to each exponent. In our case type refers to the different type of dynamics to which the particle is subjected–wall or fluid dynamics.

If λ^n is the nth exponent, the generating Lyapunov vector at time t would be $\delta\mathbf{\Gamma}_i^n(t)$, where i is the particle index. We can now introduce the normalized amplitude $\gamma_i^n(t)$ of the Lyapunov vector $\delta\mathbf{\Gamma}_i^n(t)$ (Ref. 46),

$$\gamma_i^n(t) \equiv \frac{|\delta\mathbf{\Gamma}_i^n(t)|^2}{\Sigma_{j=1}^N |\delta\mathbf{\Gamma}_j^n(t)|^2}. \tag{21}$$

As a consequence of this definition, the following conditions are satisfied:

$$\sum_{i=1}^{N} \gamma_i^n(t) = 1, \tag{22}$$

$$0 \leq \gamma_i^n(t) \leq 1. \tag{23}$$

Following Taniguchi and Morriss,[46] we can also introduce an entropy like quantity S^n defined as

$$S^n \equiv -\sum_{i=1}^{N} \langle \gamma_i^n(t) \ln\ \gamma_i^n(t) \rangle, \tag{24}$$

where $\gamma_j^n(t)$ is treated as a distribution function. The quantity W^n,

$$W^n \equiv \exp(S^n), \tag{25}$$

is the localization width of the nth Lyapunov exponent λ^n.[46] One property of the localization width which helps to clarify its physical meaning is that

$$1 \leq W^n \leq N. \tag{26}$$

The situation $W^n=1$ only occurs when a single $\gamma_i^n(t)$ is equal to one and all others are zero, while $W^n=N$ occurs when all the $\gamma_i^n(t)$ have the same value of $1/N$. It is clear at this point that the localization width quantifies the number of particles contributing to a particular Lyapunov vector and the corresponding Lyapunov exponent.

III. RESULTS

The results presented here pertain to a simulation box of 18 fluid particles at a density $\rho_F=0.6$ and two walls delimiting a channel of width $L_y=6.826$. The length of the simulation box along the x-axis is $L_x=4.180$. Each wall is formed by two layers of four atoms arranged in an fcc lattice and at a density of $\rho_W=0.8$. Since we desire an equivalent contribution to the Lyapunov spectra from the fluid and dissipative wall dynamics, a similar number of fluid and wall particles have been simulated. Also, because of the intensity of the computation task, the system size had to be kept low. Note that while the computation time for a molecular dynamics simulation increases as $O(N)$ (at best), where N is the number of particles, in the case of a calculation of the Lyapunov spectrum, the increase is $O(N^2)$ at best. The kinetic temperature is kept at a fixed value of $T=1.0$. The time step applied was $\Delta t=10^{-3}$, a simulation time of $t=100\,000$ (which is considerably longer than the thermalization time) has been used before data production and a further $t=10\,000$ for collecting the data, for a total simulation time of $t=110\,000$, corresponding to around 10^8 time steps. The two flows, Couette and Poiseuille, have been simulated using three values of driving field. For Couette flow, strain rates of $\dot{\gamma}=0.5$, $\dot{\gamma}=1.0$, and $\dot{\gamma}=2.0$ have been used, while for Poiseuille flow external forces of $F_e=0.15$, $F_e=0.3$, and $F_e=0.9$ have been employed. For each pair of systems, the total dissipation is similar. These strain rates and field strengths are all quite large,[47] and this resulted in observable anisotropy between the x and y temperature components, which in the worst case scenario is around 12%. However, this work focuses on the properties of Lyapunov spectra and high values of the dissipated energy make the phase-space characterization easier.

Since the velocity gradient is not constant for sliding boundary Couette flow near the wall and Poiseuille flow, it is not possible to use the second scalar invariant of the strain-rate tensor to compare the flows at equivalent state points, as has previously been done for Couette and elongational flows.[48,49] Instead we use the entropy production rate. We can write the Gibbs entropy as

$$S(t) = -k_B \int d\mathbf{\Gamma} f(\mathbf{\Gamma},t) \ln f(\mathbf{\Gamma},t), \tag{27}$$

where $f(\mathbf{\Gamma},t)$ is the phase-space distribution function, and its evolution will be

$$\dot{S}(t)/k_B = \langle \Lambda \rangle = -\sum_i \lambda_i = g\langle \xi \rangle > 0. \tag{28}$$

Here g is the number of degrees of freedom for the thermostatted system, $\Lambda \equiv -(\partial/\partial\mathbf{\Gamma})\cdot\dot{\mathbf{\Gamma}}$ is the (so-called) phase-space compression rate, and $\langle\xi\rangle$ is the time average of the thermostat friction coefficient. This relation has been shown to hold for homogeneous systems in nonequilibrium steady states. The fact that the average phase-space compression is always positive for nonequilibrium steady states is a key factor for understanding the irreversible behavior of such systems. A positive phase-space compression means that the phase space collapses into a multifractal strange attractor, and any trajectory in the phase space violating the second law of thermodynamics will be "pushed away" by the corresponding repellor (an object like the attractor, but characterized by reversing the time arrow).[50] Values of $\dot{\gamma}$ have been chosen for the Couette system to be consistent with previous values used in the literature,[14,16] and values of F_e have then been selected to maximize the agreement in entropy production. The entropy production is an average quantity, obtainable only once the steady state has been reached, and it cannot be imposed at the beginning of a simulation. This makes it difficult to achieve exactly the same average values. Furthermore, the relation between external force and thermostatting coefficients is not linear. However, the absolute difference between Poiseuille and Couette flows never exceeds 6% in entropy production. Values of interest for the systems considered are shown in Tables I and II. The two tables refer to the same system composition and state points (same number of fluid and wall particles and same temperature and density). Table I, however, reports results for the wall particles' phase space only, while in Table II the whole phase space

TABLE I. Summary of the results for the wall phase space for Couette and Poiseuille flows at different values of strain rate and external force, respectively. The fluid obeys Newtonian dynamics and the walls are thermostatted at $T=1.0$. The errors, in brackets, are twice the standard error of the mean of ten independent runs. The value of D_{KY} cannot be defined for large fields because the maximum subsystem exponent is negative.

Flow type	Ext. field	$\langle \dot{S} \rangle$		$-\Sigma_n \lambda_W^n$		D_{KY}		$\lambda^{\max}$		$\lambda^{\min}$	
Couette	$\dot{\gamma}=0.5$	4.061	(0.003)	4.049	(0.006)	57.82	(0.01)	0.474	(0.001)	−0.602	(0.001)
Couette	$\dot{\gamma}=1.0$	17.400	(0.007)	17.41	(0.02)	31.27	(0.02)	0.370	(0.001)	−0.914	(0.001)
Couette	$\dot{\gamma}=2.0$	100.20	(0.03)	100.34	(0.05)			−0.366	(0.001)	−2.450	(0.001)
Poiseuille	$F_e=0.15$	4.133	(0.005)	4.13	(0.01)	58.66	(0.02)	0.551	(0.001)	−0.684	(0.001)
Poiseuille	$F_e=0.3$	16.500	(0.007)	16.50	(0.01)	36.20	(0.02)	0.465	(0.001)	−0.991	(0.001)
Poiseuille	$F_e=0.9$	105.46	(0.03)	105.68	(0.06)			−0.199	(0.001)	−2.855	(0.001)

(fluid, wall, and friction coefficients) has been taken into account. As expected from theory, Eq. (28), the sum of the Lyapunov exponents is equal in magnitude to the phase space compression factor with opposite sign. This is observed when the full system is considered as well as when the wall subsystem is considered. However, a phase-space compression is present in both cases. A measure of this contraction is the Kaplan–Yorke (KY) dimension.[51] This dimension has been conjectured by Kaplan and Yorke as the effective measure of the attractor in the phase space (loosely speaking it is the dimension of a volume in the phase space that neither shrinks nor grows),

$$D_{KY} = M + \frac{\Sigma_{i=1}^{M} \lambda_i}{|\lambda_{M+1}|}, \tag{29}$$

where M is the largest integer such that $\Sigma_{i=1}^{M} \lambda_i > 0$. Clearly, the ratio of the KY dimension and the ostensible dimension (66 for the wall phase space and 138 for the total phase space for the wall thermostatted system) decreases as the driving force increases, and more heat is removed to maintain the steady state. The value of the maximum Lyapunov exponent in Table II increases as the external force increases, reflecting a more chaotic dynamics. But what is interesting is that the minimum exponent has the same absolute value, to within statistical error, as the corresponding maximum exponent. As we shall explain later this is due to the more complex dynamics of the fluid and to its Newtonian dynamics reflected in the second half of the spectra (with respect to the pair index). It is also interesting to note that, in Table I, for the two highest values of external field, $\dot{\gamma}=2.0$ and $F_e=0.9$, the maximum subsystem exponents are negative and D_{KY} cannot be defined. This result can be attributed to the extremely high external fields in conjunction with the fact that these exponents, as previously explained, are not a global property of the system.

In Figs. 2 and 3, we show the shear stress, density, temperature, and streaming velocity profiles for Couette and Poiseuille flows, respectively, for $\dot{\gamma}=2.0$ and $F_e=0.3$. The shear stress (xy component of the pressure tensor) is constant along the channel for Couette flow and roughly linear for Poiseuille flow, and the velocity profiles show slip close to the walls. The densities oscillate close to the walls revealing fluid packing, but the oscillations decrease in a region of 2σ to 3σ in the middle of the channel. The temperature profile for Poiseuille flow, however, does not show a quartic profile, a physical effect due to the channel being narrow with few particles inside it.[33] Further tests on widening the pore showed profiles in agreement with classical predictions.

In Fig. 4 we show Lyapunov spectra for a confined system at equilibrium (microcanonical for the system composed by walls and fluid). Only one pair of exponents vanishes. These are associated with the time-translational invariance of the system and, as a consequence, the conserved total energy. There is no conservation of total momentum and center of mass because of the walls. The total sum of the exponents is zero and the CPR is satisfied. It is possible to distinguish a region (low pair index) where the exponents are small (in absolute value) and a region where the exponent values increase more rapidly. As we demonstrate below, this is due to the different dynamics of the wall and fluid particles. Wall particles are tethered to a lattice and thus their behavior is less chaotic than the fluid particles, which have a wider range of accessible velocities and are free to mix in space. In Fig. 4 we also show the subsystem Lyapunov spectrum computed using Eq. (20) for the fluid particles. This has been obtained by only evolving the displacement vectors associated with the fluid phase space and thereby implicitly constraining the

TABLE II. Summary of the results for the extended wall-fluid-friction coefficient phase space for Couette and Poiseuille flows at different values of strain rate and external force, respectively. The fluid obeys Newtonian dynamics and the walls are thermostatted at $T=1.0$. The errors, in brackets, are twice the standard error of the mean of ten independent runs.

Flow type	Ext. field	$\langle \dot{S} \rangle$		$-\Sigma_n \lambda^n$		D_{KY}		$\lambda^{\max}$		$\lambda^{\min}$	
Couette	$\dot{\gamma}=0.5$	4.060	(0.002)	4.055	(0.002)	136.841	(0.001)	3.513	(0.001)	−3.513	(0.001)
Couette	$\dot{\gamma}=1.0$	17.389	(0.009)	17.40	(0.01)	133.590	(0.003)	4.167	(0.001)	−4.169	(0.001)
Couette	$\dot{\gamma}=2.0$	100.4	(0.2)	100.9	(0.5)	113.5	(0.2)	5.92	(0.01)	−5.94	(0.01)
Poiseuille	$F_e=0.15$	4.132	(0.004)	4.121	(0.008)	136.784	(0.002)	3.404	(0.001)	−3.405	(0.001)
Poiseuille	$F_e=0.3$	16.486	(0.007)	16.48	(0.02)	133.433	(0.006)	3.803	(0.001)	−3.805	(0.001)
Poiseuille	$F_e=0.9$	105.40	(0.04)	105.8	(0.2)	109.68	(0.03)	5.306	(0.002)	−5.328	(0.002)

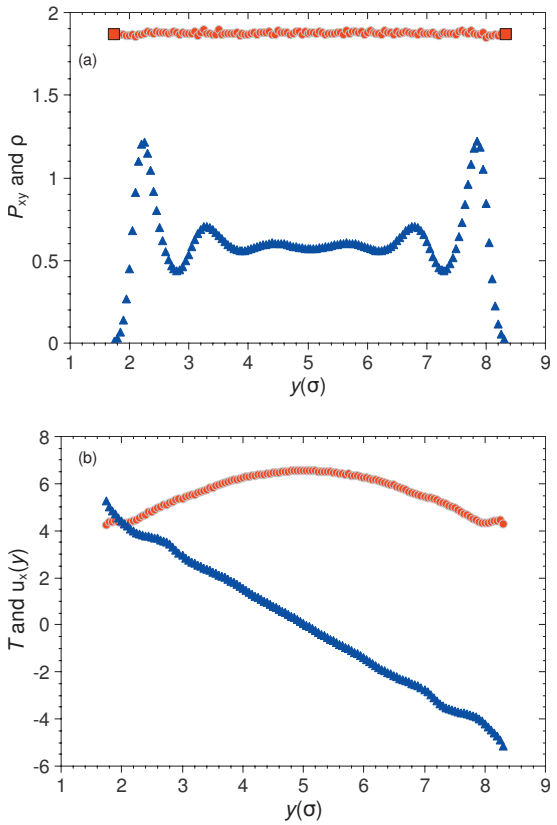

FIG. 2. Couette profiles, strain rate $\dot{\gamma}=2.0$. (a) Blue triangles: cross section density profile. Red circles: xy component of the pressure tensor P_{xy} (the big squares indicate the pressure values at the wall). (b) Blue triangles: streaming velocity. Red circles: temperature. The system consists of 18 fluid particles at a density $\rho_F=0.6$ in a channel of width $L_y=6.8\sigma$ (reduced units) and 16 wall particles at a density $\rho_W=0.8$. Walls are thermostatted at $k_BT=1.0$.

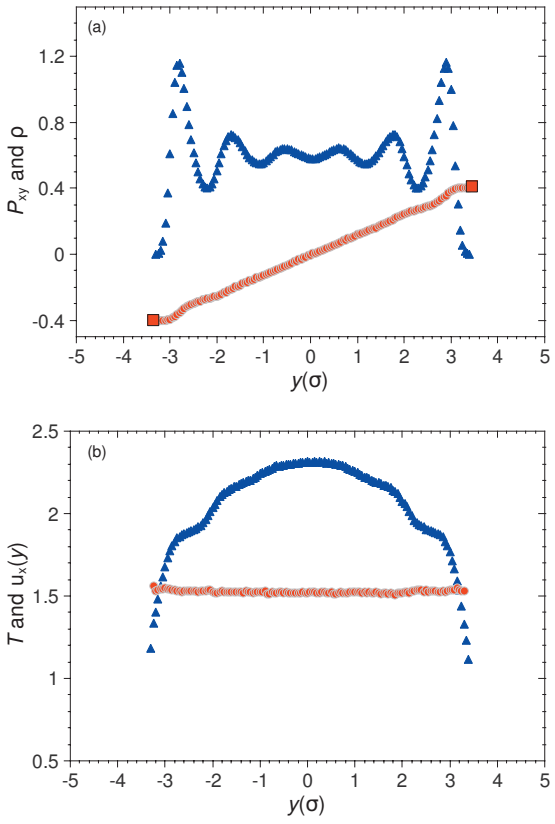

FIG. 3. Poiseuille profiles, external force $F_e=0.3$. (a) Blue triangles: cross section density profile. Red circles: xy component of the pressure tensor P_{xy} (the big squares indicate the pressure values at the wall). (b) Blue triangles: streaming velocity. Red circles: temperature. The system consists of 18 fluid particles at a density $\rho_F=0.6$ in a channel of width $L_y=6.8\sigma$ (reduced units) and 16 wall particles at a density $\rho_W=0.8$. Walls are thermostatted at $k_BT=1.0$.

Lyapunov vectors on that phase space. The interactions felt by the fluid by means of the wall particles are in some ways akin to an external force field, and if the coupling of the fluid and wall dynamics was removed (force field becomes independent of the dynamics of the fluid), this would be exact. In Fig. 4 we note that the part of the full Lyapunov spectrum with exponent index greater than 32 is very similar to the subsystem Lyapunov spectrum, indicating that those exponents are largely determined by the dynamics of the fluid. One should not expect, however, a perfect match because the dimensionality of the phase space generating the two spectra is different and contributions to the fluid exponents caused by tangent vectors involving displacements of the wall particles are prevented in the fluid exponent calculations. In recent preliminary studies we found that the spectra generated by the fluid look similar to the case in which the wall is implemented as a rigid structure without any degrees of freedom. This interesting result, however, needs to be studied further.

In Fig. 5 we show how the spectrum changes once subjected to an external field (or sliding boundaries) and where a thermostat is applied to the walls to reach the steady state. Two exponents with values close to zero are directly associated with two thermostat multipliers (see Frascoli *et al.*)[26] and are not shown in this figure or subsequent figures unless explicitly stated. Clearly the spectra are not symmetric and do not satisfy the CPR. We observe two different regions, one characterized by negative pair sum and one characterized by zero pair sum. Figure 5 also shows that there is not a large difference between Couette and Poiseuille flows, both from a qualitative and quantitative point of view: maximum exponents are slightly higher in absolute value for Couette flow.

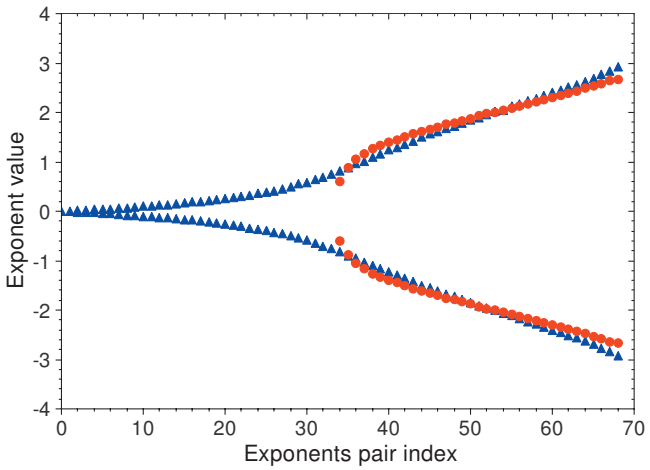

FIG. 4. Blue triangles: Lyapunov spectrum for an (*NVE*) system composed of 18 fluid and 16 wall particles. Red circles: subsystem Lyapunov spectrum for the 18 confined fluid particles only. For both spectra the fluid density is $\rho_F=0.6$ and temperature is $T=1.0$.

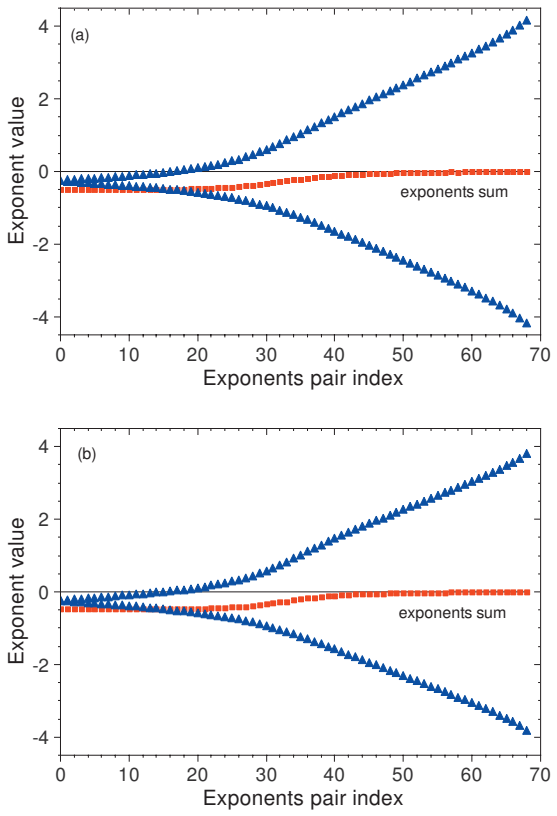

FIG. 5. (a) Lyapunov spectra for Couette flow with $\dot{\gamma}=1.0$. (b) Lyapunov spectra for Poiseuille flow with $F_e=0.3$. Both systems consist of 18 fluid particles at a density $\rho_F=0.6,16$ wall particles at a density $\rho_W=0.8$, channel width $y=6.8\sigma$, and walls thermostatted at $T=1.0$. The red squares represent the exponents' pair sum. The two zero-valued exponents associated with the thermostat multipliers are not plotted.

However, this could be due to the different value in entropy production (see Table II): a higher entropy production for Couette flow means a more chaotic spectrum than the one for Poiseuille flow.

The system is composed of particles to which a thermostat is directly applied, and others that are not, and both dissipative and conservative dynamics are observed; hence, the exponents with negative sum are largely determined by the dynamics of the wall region (the thermostatted region) while the exponents with zero sum belong to the fluid (Newtonian dynamics region). This is not trivial for two reasons: (i) the maximum Lyapunov exponents are due to the repulsive collisions (the most chaotic events) and even the wall particles could contribute when colliding with the fluid, and (ii) the contraction could be distributed along all directions in the phase space. To understand the reason for such a separation we have to consider the evolution of the displacement vector and the stability matrix.

If we consider splitting the system into wall and fluid sections and ignore the possibility of contributions from the thermostat multipliers, the phase-space displacement vector is

$$\delta\mathbf{\Gamma} = (\delta\mathbf{q}^W, \delta\mathbf{p}^W, \delta\mathbf{q}^F, \delta\mathbf{p}^F). \tag{30}$$

Its evolution is determined by the Jacobian matrix T,

$$\begin{pmatrix} \frac{\partial\dot{\mathbf{q}}^W}{\partial\mathbf{q}^W} & \frac{\partial\dot{\mathbf{q}}^W}{\partial\mathbf{p}^W} & \frac{\partial\dot{\mathbf{q}}^W}{\partial\mathbf{q}^F} & \frac{\partial\dot{\mathbf{q}}^W}{\partial\mathbf{p}^F} \\ \frac{\partial\dot{\mathbf{p}}^W}{\partial\mathbf{q}^W} & \frac{\partial\dot{\mathbf{p}}^W}{\partial\mathbf{p}^W} & \frac{\partial\dot{\mathbf{p}}^W}{\partial\mathbf{q}^F} & \frac{\partial\dot{\mathbf{p}}^W}{\partial\mathbf{p}^F} \\ \frac{\partial\dot{\mathbf{q}}^F}{\partial\mathbf{q}^W} & \frac{\partial\dot{\mathbf{q}}^F}{\partial\mathbf{p}^W} & \frac{\partial\dot{\mathbf{q}}^F}{\partial\mathbf{q}^F} & \frac{\partial\dot{\mathbf{q}}^F}{\partial\mathbf{p}^F} \\ \frac{\partial\dot{\mathbf{p}}^F}{\partial\mathbf{q}^W} & \frac{\partial\dot{\mathbf{p}}^F}{\partial\mathbf{p}^W} & \frac{\partial\dot{\mathbf{p}}^F}{\partial\mathbf{q}^F} & \frac{\partial\dot{\mathbf{p}}^F}{\partial\mathbf{p}^F} \end{pmatrix}, \tag{31}$$

where W and F refer to the wall and fluid particles, respectively.

The Jacobian matrix can be divided into four blocks relative to the wall dynamics (block 1), fluid dynamics (block 4), and wall-fluid interaction (blocks 2 and 3),

$$\left(\begin{array}{c|c} 1 & 2 \\ \hline 3 & 4 \end{array}\right),$$

where blocks 2 and 3 are null except for the terms $\partial\dot{\mathbf{p}}^W/\partial\mathbf{q}^F$ and $\partial\dot{\mathbf{p}}^F/\partial\mathbf{q}^W$. These elements are generally small compared to the terms in blocks 1 and 4, and in the case that the wall and fluid particles were uncoupled they would become zero. Therefore, the Jacobian matrix can be approximated by a symmetric block matrix. The eigenvalues of such a matrix are the collection of the eigenvalues of the diagonal blocks computed separately; this means that the spectrum is the collection of the exponents associated with the wall particles plus the ones associated with the fluid particles.

This is an interesting result because it shows the decoupling of the different dynamics occurring in the system, Newtonian for the fluid and dissipative for the walls. Unfortunately it also means that the results from the CPR and the complete characterization of the dynamics via the Lyapunov spectra cannot be achieved for an inhomogeneous system such as the confined fluid system considered here.

To test this further we now look at the full Lyapunov spectrum, the wall subsystem Lyapunov spectrum, and the fluid subsystem Lyapunov spectrum for Couette flow at $\dot{\gamma}=2.0$ in Fig. 6. Here the region of mixing is clearer as the phase-space compression is larger. If we consider the separate contributions to the spectrum from the fluid and the wall, we see that the maximal pair index exponents for the fluid and the minimal pair index exponents for the wall have approximately the same values as the maximal and minimal pair index exponents, respectively, for the total spectrum. Their union could give an approximation for the total spectrum, with the exception of the middle region where coupling of the dynamics has a large effect. This can be attributed to the quasizero off-diagonal terms in blocks 2 and 3 of Eq. (31) being nonzero.

Let us now consider the localization width for the total spectrum of the same system. We consider only the upper part of the "bell" curve that forms the Lyapunov spectrum (for symmetry reasons). The localization width provides us with a quantitative measure of the contribution of each particle species (wall or fluid) to each exponent. In the plots in Fig. 7, the x-axis refers to the exponent index, $1/2\ N\sim 0$

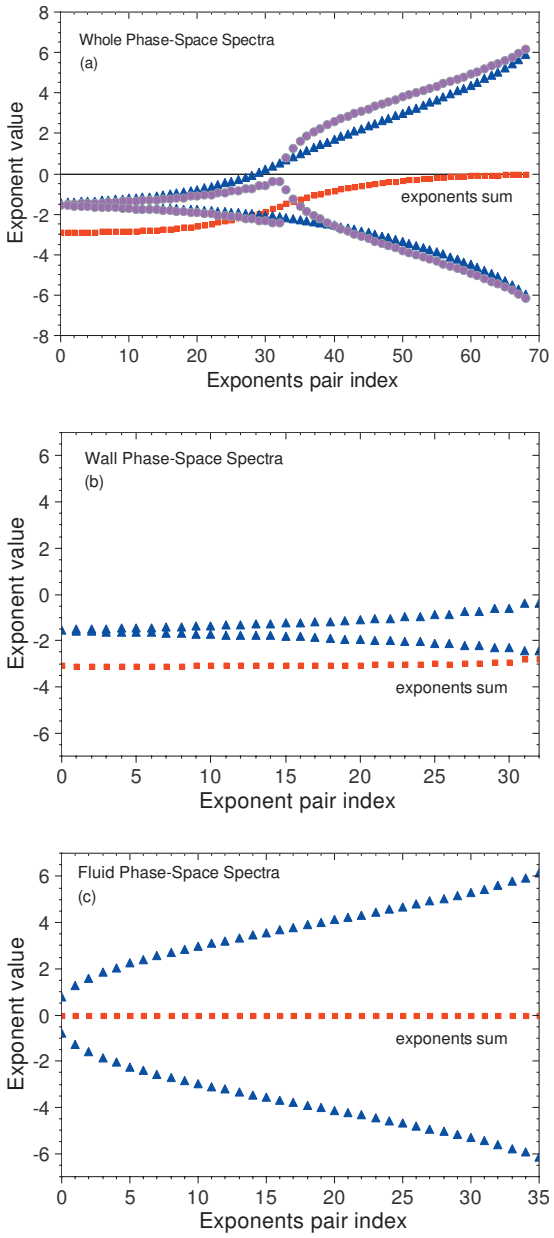

FIG. 6. Lyapunov spectra for a Couette flow system composed of 18 fluid particles at a density $\rho_F=0.6,16$ wall particles at a density $\rho_W=0.8$ with channel width $y=6.8\sigma$, strain rate $\dot{\gamma}=2.0$, and walls thermostatted at $T=1.0$ (reduced units). (a) Lyapunov spectrum computed for the whole phase space (fluid and wall, triangles); the circles are the exponents computed for the wall and fluid phase space independently. The two zero-valued exponents associated with the thermostat multipliers are not plotted. (b) Lyapunov spectrum computed for the wall phase space. (c) Lyapunov spectrum computed for the fluid phase space. The red squares represent the exponents' pair sum.

refers to λ^1, and 1 to λ^{2N}. The localization width (y-axis) has been normalized such that the sum of all contributions is equal to 1. A localization width close to 0 means that just a few particles are providing almost all of the contributions to the normalized vector associated with that particular exponent. In the plot, the triangles refer to the fluid particles' contribution that, as we can see, is maximum for high pair index exponents and minimum for low pair index exponents. The opposite behavior (minimum contribution for high pair index exponents and maximum contribution for low pair index exponents) is instead observed for the wall particles (square symbols in the plot), which confirms our interpretation of the results.

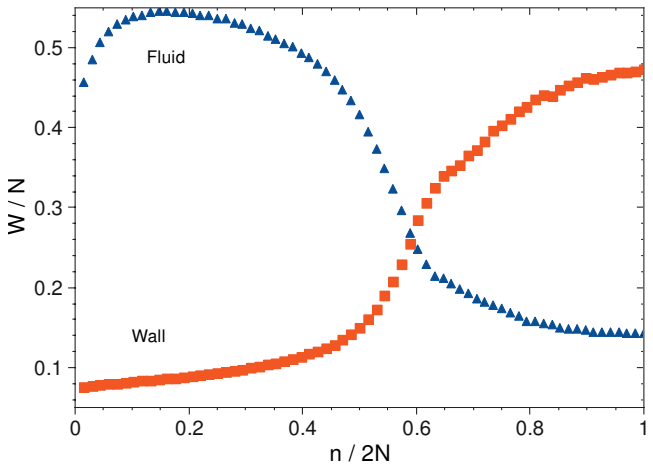

FIG. 7. Localization width for a system of 18 fluid particles and 16 wall particles. Only half of the spectrum is considered from λ^1 to λ^{2N}. Walls are thermostatted at $T=1.0$, $\rho_F=0.6$, and $\rho_W=0.8$. The contribution of the fluid particles (blue triangles) is maximum for high pair index exponents ($n/2N \simeq 0.2$) and minimum for low pair index exponents ($n/2N \simeq 1$); the opposite behavior is instead observed for the wall particles (red squares). This demonstrates that the fluid's dynamics is associated with the largest (in absolute value) exponents that sum to zero, while the wall dynamics generates the lower (in absolute value) exponents.

We now analyze the case of the wall particles' equations of motion being Newtonian and the fluid being thermostatted. This is physically an unrealistic thing to do, but it demonstrates some points more clearly. We use a profile biased thermostat (PBT),[11] so that we do not have to compute the dynamics of several friction coefficients that would have been present using a profile unbiased thermostat (PUT). To obtain the *presumed* streaming velocity, we simulate the same system thermostatted with a PUT applied to the fluid. The streaming velocity profile has been extrapolated from the linear region ($\sim 3\sigma$) in the middle of the channel with an effective value of $\dot{\gamma}=0.63$. Four plots are presented: the two in Fig. 8 are, from top to bottom, the subsystem spectrum computed separately for the wall and fluid phase space, respectively. In Fig. 9 the spectrum computed for the whole phase space is shown on the top and the subsystem exponents for the fluid and wall of Fig. 8, combined together and reordered on the bottom. Again the match is impressive, showing that the Lyapunov spectrum indeed reflects the two different dynamics, regardless of the particle species thermostatted. The exponents' sum is also in agreement in both cases: for the reordered spectrum $\Sigma\lambda=-38.3\pm0.2$ while for the whole system $\Sigma\lambda=-37.9\pm0.5$. The exponents for the wall sum to zero as expected. It is also interesting to note the steplike structure of the spectrum due to equal contributions from the walls, since they are not in contact with each other and are thermostatted independently.

Our final results refer to a Couette flow ($\dot{\gamma}=2.0$) in which fluid and walls have been thermostatted together with a PUT, shown in Fig. 10. For this purpose the simulation box has been divided into eight bins. Because each bin has a distinct friction coefficient that accounts for the different

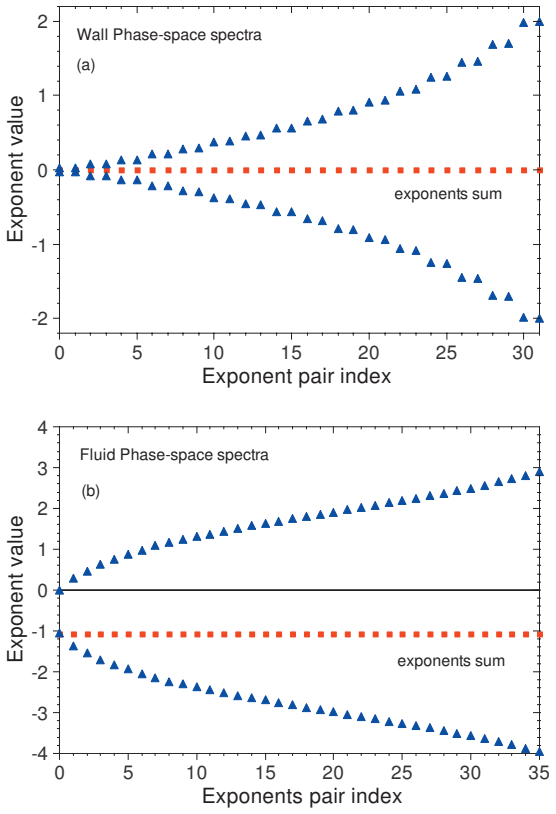

FIG. 8. (a) Lyapunov spectrum for 16 wall particles. (b) Lyapunov spectrum for 18 fluid particles. Sliding boundary method with a PBT applied to the fluid, whereas the walls are not thermostatted. Temperature $T=1.0$, density $\rho_F=0.6$, and $\rho_W=0.8$, $\dot{\gamma}=2.0$. The expected linear streaming velocity profile used in the thermostat $\dot{\gamma}=0.63$ has been extrapolated from the velocity profile of a system at the same state point with a PUT applied to the fluid. The red squares represent the exponents' pair sum.

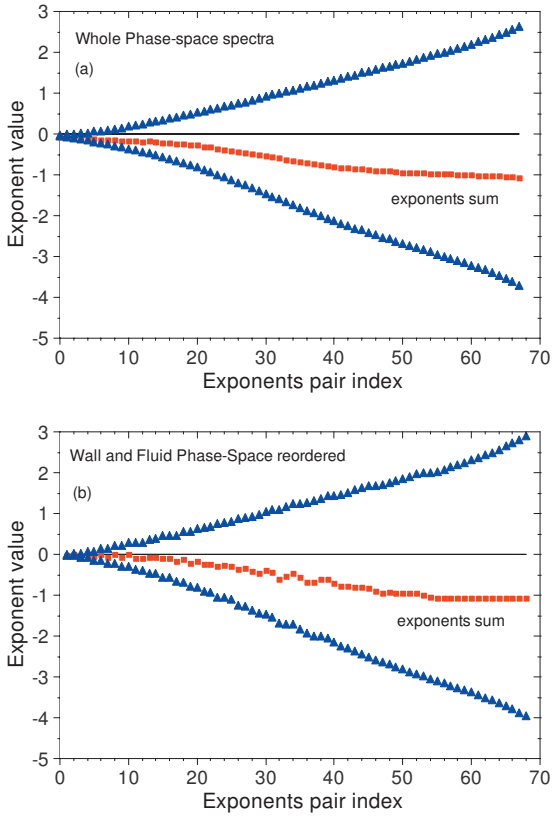

FIG. 9. (a) Lyapunov spectrum computed for the whole phase space of 18 fluid and 16 wall particles. (b) Lyapunov spectrum obtained from collecting and reordering the separate contributions of wall and fluid spectra in Fig. 8 at the same state point. The squares represent the exponents' pair sum. The zero-valued exponents associated with the thermostat multipliers are not plotted.

streaming velocity and density, the number of bins has been chosen to not excessively increase the phase-space dimension, but still account for the anisotropy of the system. The difference between the two figures is only that the exponents associated with the friction terms have not been considered in Fig. 10(a), while in Fig. 10(b) the whole phase space has been accounted for. The CPR is in this case obeyed because the contraction is distributed along all the directions in the phase space. It is interesting to see that the exponents that can be attributed to the thermostatting term in Fig. 10(b) almost vanish (indicated by the arrow), similar to what was observed by Frascoli *et al.*[26] for homogeneous isobaric systems. We refer to Sec. II A for a more comprehensive explanation.

IV. CONCLUSIONS

We studied and compared the Lyapunov spectra of inhomogeneous systems at nonequilibrium steady states for two types of flow, namely, Couette and Poiseuille. It is the first time to our knowledge that all the degrees of freedom of such dynamical systems (walls and fluid) are taken into account in this type of study. The results clearly show that, for inhomogeneous systems in steady states, the Lyapunov spectra are highly asymmetric and the CPR is not satisfied. The spectra show two distinct regions, one in which there is a negative sum of the pairs and one which tends to a zero sum. The first can be identified by the region of thermostatted particles, which are responsible for the reduction in dimensionality of the phase space, and the second by a purely Newtonian region. The existence of a few nonzero off-diagonal terms in the Jacobian matrix (due to the coupling of the dynamics of the fluid and wall particles) is the reason for the smooth mixing between the two zones.

Couette and Poiseuille flows show qualitatively the same spectra, reflecting similar chaotic properties in spite of a different distribution function. Two regions can also be distinguished in the plot of a confined fluid at equilibrium (see Fig. 4): the characteristic "bell" shape of the Lyapunov spectra is very narrow for the first half of the pair indices, indicating a small increase in the absolute value of the exponents, while the second half shows a steeper increase (the "bell" becomes wider), reflecting a much more chaotic dynamics. The narrow region can easily be identified with the wall atoms, experiencing a constrained motion since they are linked to the wall lattice, while the wider region pertains to the fluid particles where the collisions give rise to spacial reordering and mixing.

Another study considered projected Lyapunov exponents.[32] In contrast with the case when the full Lyapunov spectrum is determined and projected, we propagate a projected vector, keeping it constrained to the subspace of interest, and define a subsystem Lyapunov exponent. This allows us to obtain subsystem spectra which give

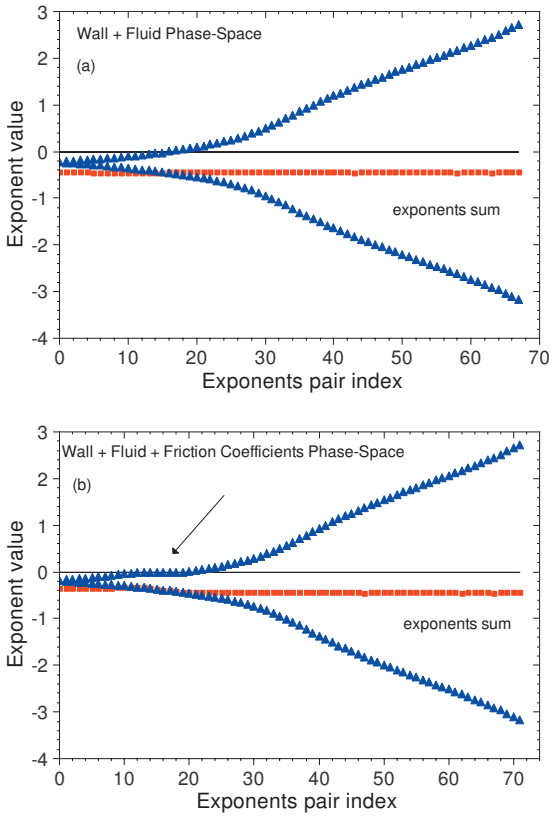

FIG. 10. Lyapunov spectra for a Couette flow system with 18 fluid particles at a density ρ_F=0.6 and 16 wall particles at a density ρ_W=0.8. Channel width y=6.8σ and strain rate $\dot{\gamma}$=2.0. The whole system is thermostatted by a PUT dividing the simulation cell in eight bins. (a) Lyapunov spectrum computed for the fluid and wall phase space. The exponents associated with the thermostat multipliers are not plotted. (b) Lyapunov spectrum computed for the fluid, wall, and friction coefficient phase space. The arrow indicates the exponents associated with the friction coefficients. The red squares represent the exponents' pair sum.

an approximation to the full spectrum. Using this approach, the part of the Lyapunov spectrum associated with the fluid (and the chaoticity of the fluid) can be determined by simply considering the evolution of displacement vectors in this subspace, which is feasible for fluids consisting of few particles that are confined between walls, without involving the possibly very large thermostatting region which could be computationally, or experimentally, impossible to determine.

Finally, we make the point that our results are independent of the particular choice of thermostatting mechanism used. In fact, we obtained very similar results for the Lyapunov spectrum of the fluid using several thermostatting schemes, including a variant of the Müller–Plathe algorithm,[52,53] where only the walls are used to induce the flow and no thermostat is used.

[1] H. A. Posch and W. G. Hoover, J. Phys.: Conf. Ser. **31**, 9 (2006).
[2] G. P. Morriss, Phys. Rev. A **37**, 2118 (1988).
[3] D. J. Evans, E. G. D. Cohen, and G. P. Morriss, Phys. Rev. Lett. **71**, 2401 (1993).
[4] D. J. Evans and D. J. Searles, Adv. Phys. **51**, 1529 (2002).
[5] O. Jepps, D. J. Evans, and D. J. Searles, Physica D **187**, 326 (2004).
[6] E. M. Sevick, R. Prabhakar, S. R. Williams, and D. J. Searles, Annu. Rev. Phys. Chem. **59**, 603 (2008).
[7] N. I. Chernov, G. L. Eyink, J. L. Lebowitz, and Y. G. Sinai, Phys. Rev. Lett. **70**, 2209 (1993).
[8] B. Moran, W. G. Hoover, and S. Bestiale, J. Stat. Phys. **48**, 709 (1987).
[9] W. G. Hoover and H. A. Posch, Chaos **8**, 366 (1998).
[10] W. G. Hoover, J. Chem. Phys. **109**, 4164 (1998).
[11] D. J. Evans and G. P. Morriss, *Statistical Mechanics of Nonequilibrium Liquids* (Cambridge University Press, London, 1990).
[12] D. J. Evans, E. G. D. Cohen, and G. P. Morriss, Phys. Rev. A **42**, 5990 (1990).
[13] E. G. D. Cohen, Physica A **213**, 293 (1995).
[14] S. Sarman, D. J. Evans, and G. P. Morriss, Phys. Rev. A **45**, 2233 (1992).
[15] D. J. Searles, D. J. Evans, and D. J. Isbister, Chaos **8**, 337 (1998).
[16] F. Frascoli, D. J. Searles, and B. D. Todd, Phys. Rev. E **73**, 046206 (2006).
[17] F. Bonetto, E. G. D. Cohen, and C. Pugh, J. Stat. Phys. **92**, 587 (1998).
[18] C. P. Dettmann and G. P. Morriss, Phys. Rev. E **53**, R5545 (1996).
[19] J. Gollub, U.S. National Committee on Theoretical and Applied Mechanics Technical Report, 2006.
[20] D. J. Evans and G. P. Morriss, Comput. Phys. Rep. **1**, 297 (1984).
[21] A. W. Lees and S. F. Edwards, J. Phys. C **5**, 1921 (1972).
[22] W. G. Hoover, D. J. Evans, R. B. Hickman, A. J. C. Ladd, W. T. Ashurst, and B. Moran, Phys. Rev. A **22**, 1690 (1980).
[23] P. J. Daivis and B. D. Todd, J. Chem. Phys. **124**, 194103 (2006).
[24] J. D. Weeks, D. Chandler, and H. C. Andersen, J. Chem. Phys. **54**, 5237 (1971).
[25] D. M. Heyes and H. Okumura, Mol. Simul. **32**, 45 (2006).
[26] F. Frascoli, D. J. Searles, and B. D. Todd, Phys. Rev. E **77**, 056217 (2008).
[27] D. Panja and R. van Zon, Phys. Rev. E **66**, 021101 (2002).
[28] W. G. Hoover, H. A. Posch, and C. G. Hoover, Chaos **2**, 245 (1992).
[29] H. A. Posch and W. G. Hoover, Phys. Rev. A **39**, 2175 (1989).
[30] K. Aoki and D. Kusnezov, Phys. Rev. E **68**, 056204 (2003).
[31] W. G. Hoover, H. A. Posch, K. Aoki, and D. Kusnezov, Europhys. Lett. **60**, 337 (2002).
[32] H. A. Posch and W. G. Hoover, Physica D **187**, 281 (2004).
[33] K. P. Travis, B. D. Todd, and D. J. Evans, Phys. Rev. E **55**, 4288 (1997).
[34] J. Casas-Vázquez and D. Jou, Rep. Prog. Phys. **66**, 1937 (2003).
[35] D. J. Evans, W. G. Hoover, B. H. Failor, B. Moran, and A. J. C. Ladd, Phys. Rev. A **28**, 1016 (1983).
[36] W. G. Hoover, Phys. Rev. A **31**, 1695 (1985).
[37] P. J. Daivis, K. P. Travis, and B. D. Todd, J. Chem. Phys. **104**, 9651 (1996).
[38] B. D. Todd and D. J. Evans, Phys. Rev. E **55**, 2800 (1997).
[39] B. D. Todd, D. J. Evans, and P. J. Daivis, Phys. Rev. E **52**, 1627 (1995).
[40] J. P. Eckmann and D. Ruelle, Rev. Mod. Phys. **57**, 617 (1985).
[41] G. Benettin, L. Galgani, A. Giorgilli, and J. M. Strelcyn, Meccanica **15**, 9 (1980).
[42] G. Benettin, L. Galgani, A. Giorgilli, and J. M. Strelcyn, Meccanica **15**, 21 (1980).
[43] I. Shimada and T. Nagashima, Prog. Theor. Phys. **61**, 1605 (1979).
[44] W. G. Hoover and H. A. Posch, Phys. Lett. A **113**, 82 (1985).
[45] I. Goldhirsch, P. L. Sulem, and S. A. Orszag, Physica D **27**, 311 (1987).
[46] T. Taniguchi and G. P. Morriss, Phys. Rev. E **68**, 046203 (2003).
[47] K. S. Mriziq, M. D. Dadmun, and H. D. Cochran, Rheol. Acta **46**, 839 (2007).
[48] R. B. Bird, R. C. Armstrong, and O. Hassager, *Dynamics of Polymeric Liquids* (Wiley, New York, 1987).
[49] P. J. Daivis, M. L. Matin, and B. D. Todd, J. Non-Newtonian Fluid Mech. **111**, 1 (2003).
[50] D. J. Evans, D. J. Searles, W. G. Hoover, C. G. Hoover, B. L. Holian, H. A. Posch, and G. P. Morriss, J. Chem. Phys. **108**, 4351 (1998).
[51] J. L. Kaplan and J. A. Yorke, *Chaotic Behaviour of Multidimensional Difference Equation* (Springer, Berlin, 1979).
[52] F. Müller-Plathe, Phys. Rev. E **59**, 4894 (1999).
[53] P. Bordat and F. Müller-Plathe, J. Chem. Phys. **116**, 3362 (2002).